

Tuning the Electronic, Optical, and Magnetic Properties of Monolayer GaSe with a Vertical Electric Field

Congming Ke,¹ Yaping Wu,^{1,*} Guang-Yu Guo,^{2,3,†} Wei Lin,¹ Zhiming Wu,¹ Changjie Zhou,⁴ and Junyong Kang¹

¹*Department of Physics, OSED, Fujian Provincial Key Laboratory of Semiconductor Materials and Applications, Xiamen University, Xiamen, 361005, China*

²*Department of Physics, National Taiwan University, Taipei 10617, Taiwan*

³*Physics Division, National Center for Theoretical Sciences, Hsinchu 30013, Taiwan*

⁴*Department of Physics, School of Science, Jimei University, Xiamen 361021, China*



(Received 28 September 2017; revised manuscript received 26 January 2018; published 20 April 2018)

Inspired by two-dimensional material with their unique physical properties and innovative device applications, here we report a design framework on monolayer GaSe, an important member of the two-dimensional material family, in an effort to tune the electronic, optical, and magnetic properties through a vertical electric field. A transition from indirect to direct band gap in monolayer GaSe is found with an electric field of 0.09 V/Å. The giant Stark effect results in a reduction of the band gap with a Stark coefficient of 3.54 Å. Optical and dielectric properties of monolayer GaSe are dependent on the vertical electric field. A large regulation range for polarization $\mathbf{E} \parallel \hat{\mathbf{c}}$ is found for the static dielectric constant. The optical anisotropy with the dipole transition from $\mathbf{E} \parallel \hat{\mathbf{c}}$ to $\mathbf{E} \perp \hat{\mathbf{c}}$ is achieved. Induced by the spin-orbit coupling, spin-splitting energy at the valence band maximum increases linearly with the electric field. The effective mass of holes is highly susceptible to the vertical electric field. Switchable spin-polarization features in spin texture of monolayer GaSe are predicted. The tunable electronic, optical, and magnetic properties of monolayer GaSe hold great promise for applications in both the optoelectronic and spintronic devices.

DOI: [10.1103/PhysRevApplied.9.044029](https://doi.org/10.1103/PhysRevApplied.9.044029)

I. INTRODUCTION

As a real two-dimensional (2D) material, graphene with a cornucopia of enticing properties, is well recognized as a promising candidate for next-generation nanoelectronics [1–4]. However, the lack of an intrinsic band gap and the weak spin-orbit coupling (SOC) strength are major obstacles for developing optoelectronic and spintronic devices [5,6]. Recently, a new kind of layered semiconductor material, group IIIA metal monochalcogenides MX ($M = \text{Ga, In}$; $X = \text{S, Se, Te}$) has received a lot of attention, because of their superior performance in the field of optoelectronics and spintronics [7–9]. Especially, mechanical exfoliated GaSe nanoslab shows an excellent optoelectronic property with a photoresponsivity of 2.8 A/W [10], external quantum efficiency of 1367% [9], and an on:off ratio of 10^3 [11]. It is of high interest that GaSe is demonstrated to generate and preserve a high degree of spin polarization exceeding 90% under nonresonant optical pumping, superior to traditional GaAs and transition-metal dichalcogenides [12–15]. An accurate control of these properties is considered critical to satisfying the multiple

demands of device design. Strain engineering [16], surface decoration [17], and nonequilibrium doping [18,19] have been proven as being effective routes to tune the electronic and spin behaviors of GaSe materials. For instance, the electronic properties of GaS/GaSe van der Waals heterostructures can be continuously tuned by an external strain [20]; half-metallicity with 100% spin polarization is achieved in monolayer GaSe by adsorbing the Fe atoms [17]; itinerant ferromagnetism as well as the half-metallicity can also be generated in monolayer GaSe by hole doping or selective doping with specific atoms [18]. It is widely held that the band structure is generally sensitive to the external electric field [21]. Compared with the above-mentioned techniques, the control process can be simplified by employing a reversible external electric field, without bringing in additional lattice deformation or damage which generally reduces the carrier mobility in the material. The considerable SOC effect in GaSe further provides a possibility for an all-electric control technique, possessing higher compatibility with modern microelectronic devices. In light of the advantages mentioned above, the modulation of the electronic, optical, and magnetic properties of monolayer GaSe by an electric field is of great significance.

In this work, we study the modulation of the electronic, optical, and magnetic properties of monolayer GaSe

*ypwu@xmu.edu.cn

†gyguo@phys.ntu.edu.tw

through first-principles density function calculations. The investigation is initiated with the dependence of anisotropy for the optical and the dielectric properties on the vertical electric field. The tunable effective mass of holes and its possible implications are studied. By analyzing the spin-projected band structure, we explore the physical mechanism of the influence of the vertical electric field to the spin textures. The present work provides a general theoretical background and a well-founded guideline to stimulate experimental characterization and fabrication of the tunable 2D optoelectronic and spintronic devices.

II. THEORY AND COMPUTATIONAL METHOD

A. Geometry and electronic structure determination

Atomic and electronic structures of monolayer GaSe with and without an applied electric field are calculated based on the density functional theory (DFT) with the generalized gradient approximation (GGA). The accurate projector-augmented wave method, as implemented in the Vienna *ab initio* simulation package (VASP) [22–24] code, is used. A slab model with a 1×1 unit cell and a 20-Å vacuum layer along the z direction is constructed. The valence electron configurations of Ga and Se atoms adopted are $3d^{10}4s^24p^1$ and $4s^24p^4$, respectively. The GGA [25] with Perdew-Burke-Ernzerhof (PBE) [26] parametrization is employed as the exchange-correlation functional. Electron wave functions are expanded in plane waves with an energy cutoff of 360 eV. The Brillouin zone is sampled with a $31 \times 31 \times 1$ Monkhorst-Pack grid of k points. For each applied electric field strength, all atomic degrees of freedom, including lattice constants, are fully relaxed with self-consistent convergence criteria of 0.01 eV/Å and 10^{-6} eV for the atomic forces and total energy, respectively.

B. Calculation of optical properties

The imaginary part of the dielectric function $\epsilon''_{\alpha\alpha}(\omega)$ due to direct interband transitions is calculated by using the Fermi golden rule [27],

$$\epsilon''_{\alpha\alpha}(\omega) = \frac{4\pi^2 e^2}{\Omega} \lim_{q \rightarrow 0} \frac{1}{q^2} \sum_{c,v,k} 2\omega_k \delta(\epsilon_{ck} - \epsilon_{vk} - \omega) \times \langle \mu_{ck} + e_{\alpha} q | \mu_{vk} \rangle \langle \mu_{ck} + e_{\alpha} q | \mu_{vk} \rangle^*.$$

Here, the indices c , v , μ_k , ω_k , Ω , and e_{α} refer to the conduction band states, the valence band states, the eigenstate with wave vector \mathbf{k} , the k -point weights (which are defined such that they sum to 1), the effective volume [$(\sqrt{3}/2)a^2 h_{\text{eff}}$, $h_{\text{eff}} = 7.959$ Å] [28], and the unit vectors for the three Cartesian directions, respectively. A factor of 2 is multiplied to the weights for considering the spin-degenerate system. And the real part of the dielectric tensor is obtained by performing the Kramers-Kronig transformation [29]:

$$\epsilon'_{\alpha\alpha}(\omega) = 1 + \frac{2}{\pi} P \int_0^{\infty} \frac{\epsilon'_{\alpha\alpha}(\omega') \omega'}{\omega'^2 - \omega^2} d\omega'.$$

Absorption coefficient $[A(\omega)]$ and refractive index $[n(\omega)]$ are computed by taking the real and imaginary parts of the dielectric tensor $\epsilon_{\alpha\alpha}(\omega)$ in terms of the equations given below [30,31]:

$$A(\omega) = \left(\frac{\sqrt{2}\omega}{c} \right) \{ [\epsilon'_{\alpha\alpha}(\omega) + \epsilon''_{\alpha\alpha}(\omega)]^{1/2} - \epsilon'_{\alpha\alpha}(\omega) \}^{1/2},$$

$$n(\omega) = \left(\frac{1}{\sqrt{2}} \right) \left[\sqrt{\epsilon'_{\alpha\alpha}(\omega) + \epsilon''_{\alpha\alpha}(\omega)} + \epsilon'_{\alpha\alpha}(\omega) \right]^{1/2}.$$

In the present calculations, we use an effective unit cell volume of monolayer GaSe instead of the volume of the supercell which is arbitrary. It is well known that the GGA ignores the many-body effects, leading to the underestimate of the band gap [32]. To obtain more accurate band structure, we introduce the scissors correction to amend the band gap of GGA to the band gap of Heyd-Scuseria-Ernzerhof (HSE06) [33].

III. RESULTS AND DISCUSSION

A. Band structures

The equilibrium geometric configuration of monolayer GaSe is shown in Fig. 1(a). After full relaxation, its planar projection exhibits nearly a perfect hexagonal honeycomb structure, similar to that of graphene and conventional 2D nanomaterials [34]. Equilibrium lattice constant of GaSe is 3.75 Å, and the lengths of Ga–Ga and Ga–Se bonds are both ~ 2.47 Å, well consistent with the reported values in the literature [35]. Without the electric field, monolayer GaSe exhibits an indirect band-gap band structure which has the conduction band minimum (CBM) at the Γ point and the valence band maximum (VBM) close to the Γ point along the Γ - K direction, as shown in Fig. 1(b).

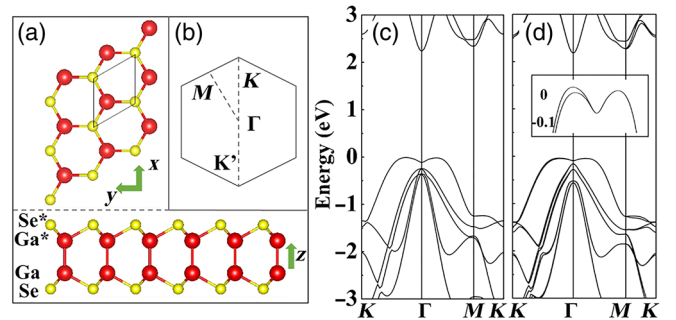


FIG. 1. (a) Top and side views of the atomic configuration of monolayer GaSe, where the rhombus indicates a unit cell. (b) Brillouin zone. (c) and (d) Band structure of monolayer GaSe without and with the consideration of spin-orbit coupling, respectively. In (d), the inset shows the enlarged valence bands near the Γ point.

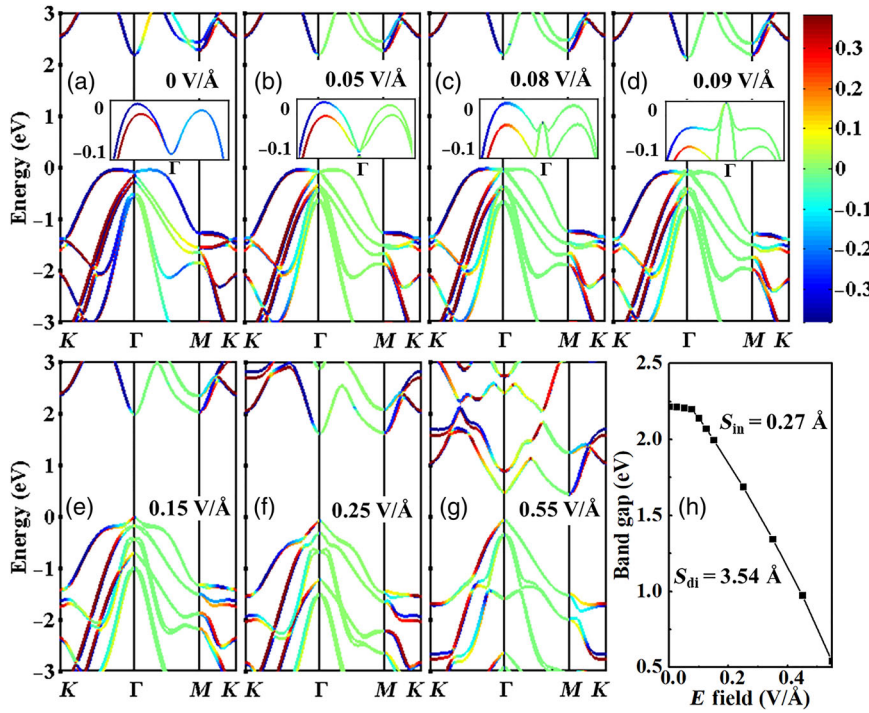


FIG. 2. (a)–(g) Spin-projected energy bands of monolayer GaSe with different electric fields of 0, 0.05, 0.08, 0.09, 0.15, 0.25, and 0.55 V/Å, respectively. Red and blue colors mean the up and down spins, respectively. (h) Band-gap E_g versus the applied electric field E for monolayer GaSe. S_{in} (at 0.05 V/Å) and S_{di} (at $E = 0.25$ V/Å) denote the giant Stark effect coefficient for the indirect-gap and direct-gap regions, respectively.

The calculated band gap is 2.22 eV, which turns out to be 3.17 eV in the HSE06 calculation. The topmost valence band has an interesting Mexican-hat-like energy dispersion, where the energy maximum along the Γ -K direction (denoted as VBM) is slightly higher (~ 0.01 eV) than that along the Γ -M direction (denoted as VBM*). The special band structure gives rise to a van Hove singularity in the density of states, indicative of an abundant tunability of the electronic properties [18]. Taking into account the SOC effect, all the bands along the Γ -K direction show a small spin splitting. The calculated splitting energy of the VBM is about 11.2 meV. However, for the Γ -M direction, the bands are spin degenerate, due to their symmetry in the Brillouin zone.

The evolution of the band structure in the presence of a vertical external electric field is shown in Figs. 2(a)–2(g). The topmost valence band at the Γ point rises continuously, accompanied with the falling of the conduction band. As the topmost valence band at the Γ point finally surpasses both the VBM and VBM*, i.e., a transformation from the indirect to direct band gap occurs in monolayer GaSe, which implies a greater luminous efficiency modulated by the vertical electric field. Simultaneously, the variation of the band edges gives rise to the reduction of the band gap. Figure 2(h) summarizes the calculated band gap versus the applied electric field. When the applied electric field is smaller than ~ 0.1 V/Å, the band structure has an indirect band gap and the response of the band gap to the electric field is dull. Interestingly, as the electric field is further increased, the band gap becomes direct and it exhibits a monotonic decrease with the increasing field [see Fig. 2(h)]. The behavior of the band structure suggests

a typical giant Stark effect, and the linear giant Stark effect coefficient S satisfies the following relation [36]:

$$\frac{dE_g}{dE} = -eS,$$

where e is the electron charge. For the indirect-gap and direct-gap regions, the deduced giant Stark effect coefficients are 0.27 and 3.54 Å, respectively. Given the linear giant Stark effect, monolayer GaSe would become metallic when the vertical electric field is increased to 0.71 V/Å. This critical electric field for the semiconductor-to-metal transition would be increased to 0.98 V/Å in the hybrid functional HSE06 calculation.

To gain a deep insight into the changes in the band structure of monolayer GaSe modulated by the vertical electric field, the atomic-orbital-projected band structures, as well as the spatial distributions of the partial charge densities at CBM and VBM are displayed in Figs. 3 and 4, respectively. For monolayer GaSe without the electric field, the atomic orbitals of the upper ($\text{Ga}^* s$, $\text{Se}^* s$, $\text{Se}^* p_x$, $\text{Se}^* p_y$, and $\text{Se}^* p_z$) and the lower sublayers ($\text{Ga} s$, $\text{Se} s$, $\text{Se} p_x$, $\text{Se} p_y$, and $\text{Se} p_z$) contribute equally to the band structure. The CBM is mainly generated from $\text{Ga} s$ ($\text{Ga}^* s$) and $\text{Se} s$ ($\text{Se}^* s$) orbitals tightly located around the Ga (Ga^*) and Se (Se^*) atoms in a spherical shape. The VBM mainly originates from the $\text{Se} p_z$ ($\text{Se}^* p_z$) orbitals that look like a dumbbell shape along the z direction. $\text{Se} p_x$ and $\text{Se} p_y$ orbitals are distributed below the topmost valence band while the states near the Γ point are coupled. When applying a vertical electric field, the potential of the upper sublayer is lifted while that of the lower sublayer is

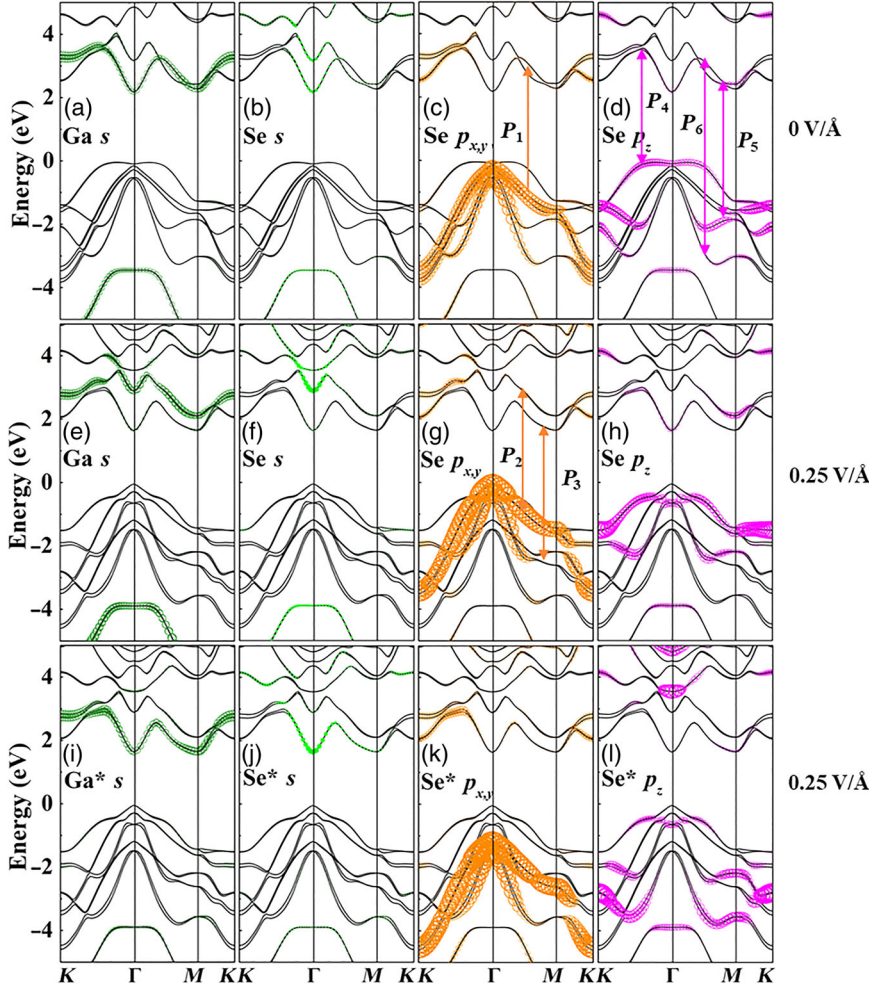


FIG. 3. Atomic orbital projected band structures of monolayer GaSe (a)–(d) without the electric field and (e)–(l) with an electric field of 0.25 V/\AA . The black curves are the overall band structures. The colored circles represent the projection of Ga (Ga^*) and Se (Se^*) atomic orbitals, and the size of the circles indicates the corresponding orbital weight.

depressed. Thus, a potential difference between the two sublayers is created, resulting in a Stark splitting in the band structure and a shrink of the band gap. Partial charge densities tune into an asymmetrical distribution between the two sublayers, especially for the CBM, as seen in Fig. 4(b), and more states accumulate in the lower sublayer. With the external electric field (such as 0.25 V/\AA in Fig. 3) higher than the critical value, the CBM is more contributed by the s orbital of the upper Ga^* and Se^* atoms than that of the lower atoms, while the VBM is dominated by hybridized p_x and p_y orbitals of the lower Se atoms instead of the original p_z orbital of all Se (Se^*) atoms. Correspondingly, initial dumbbell-shaped spatial charge densities are regulated from parallel to perpendicular to the z direction, as shown in Fig. 4(c). Consequently, the diminution of the band gap and the formation of the direct band-gap structure of monolayer GaSe result from the significant subband mixing caused by the perturbation of the external electric field.

B. Optical properties

An examination of the valence band suggests a preferred dipole selection of the electron transition from the z to xy polarization, and this implies a controllable anisotropy

under the vertical electric field. To further address this interesting issue, the complex dielectric function versus the applied electric field is calculated. As seen in Figs. 5(a) and 5(c), the imaginary part of the dielectric function has different absorption behaviors for the polarized lights with $\mathbf{E} \perp \hat{\mathbf{c}}$ and $\mathbf{E} \parallel \hat{\mathbf{c}}$, revealing a profound optical anisotropy in monolayer GaSe. In the absence of an external electric field, the dipole transition shows an $\mathbf{E} \parallel \hat{\mathbf{c}}$ preference, with a 0.1-eV energy difference of the absorption edges. As an external electric field is applied, the absorption edges of the polarized lights with both $\mathbf{E} \parallel \hat{\mathbf{c}}$ and $\mathbf{E} \perp \hat{\mathbf{c}}$ shift to lower energies, and the energy difference decreases. A reversal of the dipole transition from $\mathbf{E} \parallel \hat{\mathbf{c}}$ to $\mathbf{E} \perp \hat{\mathbf{c}}$ anisotropy occurs at $E = 0.14 \text{ V/\AA}$ (at $E = 0.08 \text{ V/\AA}$, if the SOC is taken into account).

The evolution mechanism of the optical anisotropy of monolayer GaSe can be understood in terms of the atomic orbital-projected band structures in Fig. 3 and spatial distribution of the partial charge in Fig. 4. The CBM is mainly contributed by the hybridized s and p_z orbital of Ga atoms, while the VBM is derived from p_z orbital of Se atom at lower electric fields and from the mixture of p_x and p_y components as the external electric field is increased to the

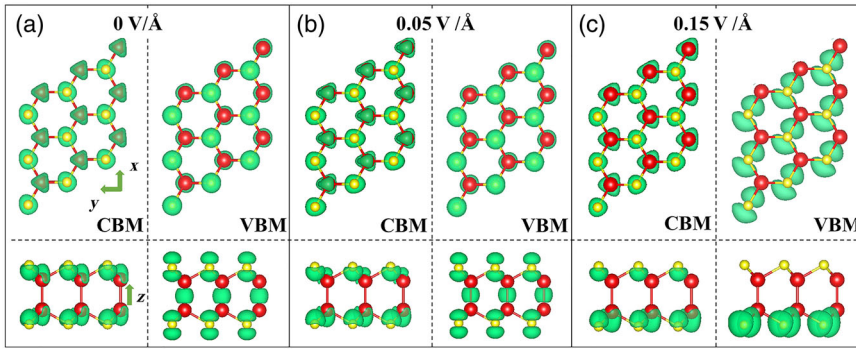


FIG. 4. (a)–(c) Partial charge densities of the states at CBM and VBM of monolayer GaSe with the electric fields of 0, 0.05, and 0.15, respectively. The value of the green isosurfaces of the partial charge densities is $0.009 \text{ e}\text{\AA}^{-3}$.

critical value and beyond. According to the dipole selection rules [37], the transition from a valence band to a conduction band in monolayer GaSe is favorable for the $\mathbf{E} \parallel \hat{c}$ polarized light with the external electric field from 0 to 0.08 V/\AA . However, it becomes available for the $\mathbf{E} \perp \hat{c}$ polarized light as the external electric field is further increased.

The main peaks in the absorption spectra (i.e., the imaginary part of the dielectric function) as labeled $P_1 \sim P_6$ in Figs. 5(a) and 5(c) could be assigned to the principal interband transitions depicted in Figs. 3(c), 3(d), and 3(g). This is achieved by fitting the energies of the $P_1 \sim P_6$ peaks in Fig. 5 with that of the interband transitions in Fig. 3 and also taking the dipole selection rules into account. The principal transitions are denoted by the yellow and pink arrows in Fig. 3. For $P_1 \sim P_3$, the light polarization is of $\mathbf{E} \perp \hat{c}$ and hence the transitions come predominantly from the valence band of the Se $p_{x,y}$ orbital to the conduction band of the Ga s orbital, as indicated in Figs. 3(c) and 3(g). For $P_4 \sim P_6$, on the other hand, the polarization is of $\mathbf{E} \parallel \hat{c}$, the transitions come mostly from the Se p_z orbital states to Ga s orbital states [see Fig. 3(d)]. These assignments

explain that peak P_1 splits into peaks P_2 and P_3 when a vertical electric field is applied, which causes the splitting of Se $p_{x,y}$ orbital dominant valence bands [see Figs. 3(c), 3(g), and 3(k)].

Similar to the imaginary part, the features in the real part of the dielectric function also shift to lower energy values with the increasing electric field, as depicted in Figs. 5(b) and 5(d). Compared with the real part for the $\mathbf{E} \perp \hat{c}$ polarization, the real part for the $\mathbf{E} \parallel \hat{c}$ polarization near the band-gap edge is found to be more visibly affected by the external electric field. Figure 6 shows the static dielectric property of monolayer GaSe, which is extracted from the real part of the dielectric function in the limit of $\omega = 0$. The intrinsic static dielectric constants for $\mathbf{E} \perp \hat{c}$ and $\mathbf{E} \parallel \hat{c}$ are 5.5 and 4.9, respectively. As the electric field is increased from 0 to 0.55 V/\AA , the static dielectric constant is enhanced from 4.9 to 6.09 for $\mathbf{E} \parallel \hat{c}$, but hardly changes for $\mathbf{E} \perp \hat{c}$. We observe that the tunable static dielectric constants arise from the rearrangement of the partial charge densities of the system caused by the applied electric field. It is known that, in classical atomic models, negative electron clouds surrounding a positive point charge

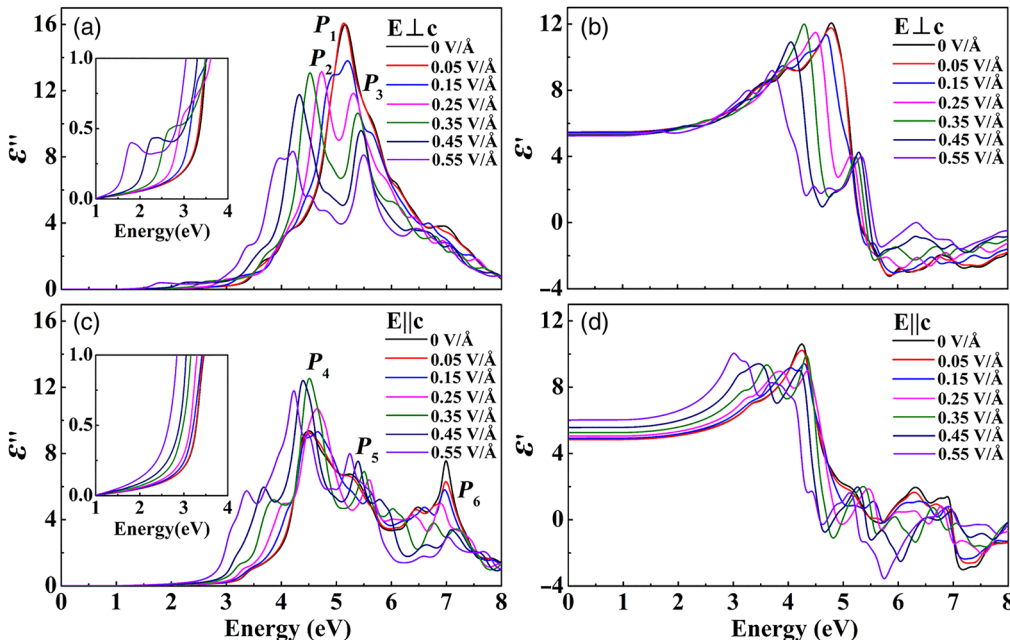


FIG. 5. Calculated optical dielectric function of monolayer GaSe versus the applied electric field. The imaginary parts are displayed in (a) and (c). The real parts are plotted in (b) and (d). Upper panels (a) and (b) are for the in-plane polarization ($\mathbf{E} \perp \hat{c}$). Lower panels are for the perpendicular polarization ($\mathbf{E} \parallel \hat{c}$). The inset in (a) and (c) shows the enlarged absorption spectra.

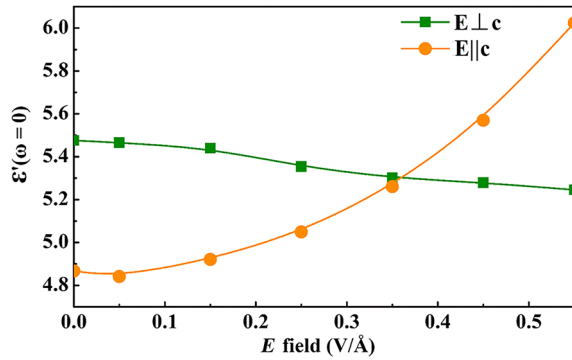


FIG. 6. Static dielectric constant of monolayer GaSe versus the applied electric field.

distribute symmetrically. Once they are combined to form a material, the interaction between atoms distorts the electron cloud and thus produces the electronic polarization. In the presence of the electric field, the charge cloud is further distorted with the partial charge densities turning into an asymmetrical distribution between the two sublayers [Fig. 4(b)], which promotes the electronic polarization. The optical and dielectric anisotropy of monolayer GaSe and its modulation by the vertical electric field promises wide possibilities for engineering and harnessing the 2D optoelectronic devices.

We should point out that in this work, the optical properties are calculated based on the independent-particle approximation within DFT-GGA, i.e., the many-body effects, namely, the quasiparticle self-energy corrections and excitonic effects, are neglected. These many-body effects on the optical properties of 2D systems such as MoS₂ and SiC, monolayers [32,38] are especially pronounced due to quantum confinement. Nevertheless, the self-energy corrections are taken into account here by the scissors correction using the band gaps from the hybrid functional HSE06 [33] calculations, as mentioned above in Sec. II B. Weak or moderate electron-hole interaction would enhance the peaks near the absorption edge [39]. However, strong electron-hole interaction in, e.g., monolayer MoS₂, could give rise to additional prominent excitonic peaks below the absorption edge [32]. Nonetheless, in contrast to the 1H-transition metal dichalcogenide semiconductor monolayers, monolayer GaSe has an indirect band gap and, hence, one could expect no bright excitonic peak below the absorption edge. Indeed, no excitonic transition peak is observed in ultrathin GaSe films in a very recent experiment [40]. In short, taking into account the many-body effect such as electron-hole interaction would not be expected to significantly alter the optical properties reported in this paper.

C. Spin-orbit coupling and spin texture

As has been mentioned above, when considering the SOC effect, the bands along the Γ - K direction show a spin

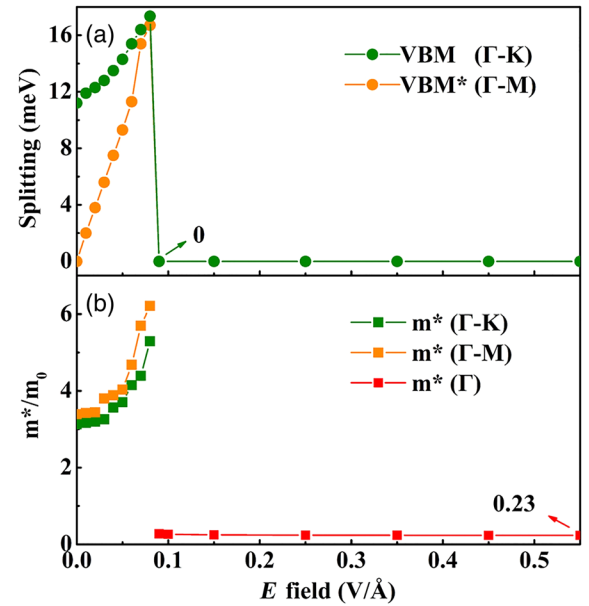


FIG. 7. (a) Spin-splitting energy of VBM and VBM* as a function of applied electric field. (b) Electric field dependence of the effective mass.

splitting while those along the Γ - M direction are degenerate without the external electric field. The spin splitting is found to be significantly dependent on the electric field, as seen in the spin-projected energy bands in Figs. 2(a)–2(d). With the increasing electric field from 0 to 0.08 V/Å, the VBM exhibits a linearly increased splitting with the splitting energy varying from 11.2 to 17.3 meV, as shown in Fig. 7(a). Compared with the VBM along the Γ - K direction, the VBM* along the Γ - M direction is even more sensitive to the external electric field, which becomes split under the electric field. The splitting energy reaches about 16.7 meV at 0.08 V/Å, being close to the value for the VBM. When the electric field exceeds 0.09 V/Å, the VBM becomes located at the Γ point and is spin degenerate instead.

Since the vertical electric field can dramatically change the curvature of the band structure, the effective masses of holes can be also regulated by the electric field. Figure 7(b) shows the effective masses as a function of the applied electric field, which are calculated using the relation $m^* = \hbar^2 / (\partial^2 E / \partial k^2)$ for the k points located closely to the corresponding VBM and VBM*. When the vertical electric field changes from 0 to 0.08 V/Å, the effective masses of holes along the Γ - K (Γ - M) direction increase from 3.13 m_0 (3.39 m_0) to 5.29 m_0 (6.21 m_0). When the electric field exceeds 0.09 V/Å, the VBM is located at the Γ point. Consequently, the hole effective mass abruptly drops to 0.27 m_0 and reaches the minimum value of 0.23 m_0 at 0.55 V/Å (where m_0 is the free-electron mass). This small effective mass implies an outstanding carrier mobility and hence a significant promotion of the conductivity.

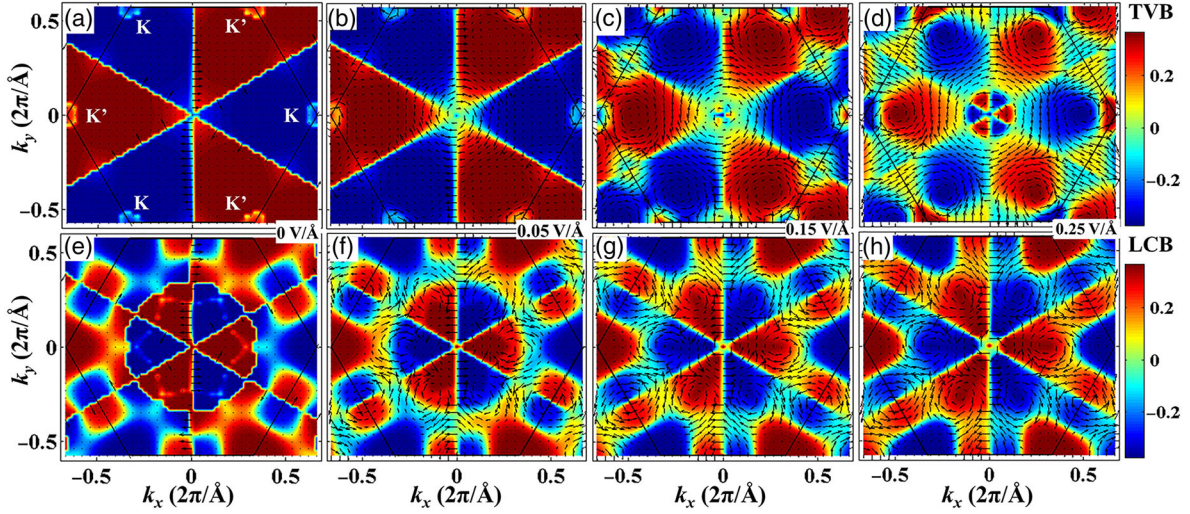


FIG. 8. Spin textures for the topmost valence band (denoted as TVB in the figure) and the lowest conduction band (denoted as LCB in the figure) of monolayer GaSe with various electric fields of (a),(e) 0 V/Å; (b),(f) 0.05 V/Å; (c),(g) 0.15 V/Å; and (d),(h) 0.25 V/Å, respectively. The arrows indicate the in-plane orientation of spin, and the color background denotes the z component of the spin. Red and blue colors indicate the up and down spins, respectively.

The SOC opens up an effective route to manipulate the spin-electronic properties of monolayer GaSe through an all-electric control method, as demonstrated by the spin textures of the topmost valence band and lowest conduction band under different electric fields in Fig. 8. In all cases, the spin possesses a threefold rotational symmetry, being consistent with the underlying symmetry of the atomic structure. Without the electric field [Figs. 8(a) and 8(e)], the z components of the spin for the lowest conduction band (LCB) and topmost valence band (TVB) near the Γ point show opposite directions. The in-plane components are nonzero only in the Γ - M directions, and they form dilute swirl-like patterns with the clockwise and anticlockwise chirality in the TVB and LCB, respectively. When applying an electric field of 0.05 V/Å [Fig. 8(b)], additional in-plane spin components in the TVB arise in other part of the Brillouin zone and they all together form a profound swirl centered at the Γ point with the clockwise chirality. All the in-plane spin components are related to the Se p_z orbital in the band structure in Fig. 2(b). Interestingly, when the electric field is increased to 0.15 V/Å [Fig. 8(c)], the big swirl splits into several vortices and the spin chirality of the central vortex is switched from the clockwise to anticlockwise at k points close to the Γ point where the (Se p_x)/ p_y orbitals overlap with the Se p_z orbital. Furthermore, the z components of the spin at the K and K' points become opposite to each other. The correlation between the chirality and the Se orbitals suggests that the reversion of the chirality originates from the hybridization between the elevated (Se p_x)/ p_y orbitals and the declined Se p_z orbital. With a further rise of the (Se p_x)/ p_y orbitals and fall of the Se p_z orbital, the orbital hybridization occurs at larger k points. Therefore, as the electric field is increased

to 0.25 V/Å [Fig. 8(d)], the anticlockwise in-plane spin components outspread, accompanied with the recovery of some clockwise in-plane components and the flip of the z component in vicinity of the Γ point at the TVB. The spin texture in the LCB is less sensitive to the external electric field compared with that of the TVB. Given that the LCB is dominated by s orbitals of Ga and Se atoms which have an even parity, the LCB is rather insensitive to the electric field. Therefore, the observed change of the spin magnitude and chirality near the Γ point can be attributed to the contribution from the valence band. These interesting phenomena show electric-controllable spin-polarization features in the spin texture of monolayer GaSe, and this promises interesting applications in spintronic devices such as spin transistors and spin light-emitting diodes [41,42].

IV. CONCLUSION

In this work, electric field dependent electronic, optical, and magnetic properties of monolayer GaSe have been investigated based on the first-principles DFT calculations. The evolution of the band structure reveals a transition from indirect to direct band gap in monolayer GaSe with an increasing vertical electric field. A monotonic decrease of the energy gap is found due to the giant Stark effect with a Stark coefficient of 3.54 Å. An optical anisotropy for the dipole transition is tuned from $\mathbf{E} \parallel \hat{c}$ to $\mathbf{E} \perp \hat{c}$, and a large regulation range is achieved for the static dielectric constant. Because of the SOC effect, the spin splitting at VBM increases linearly from 11.2 to 17.3 meV with the increasing electric field. The effective mass of holes can be tuned to as low as 0.23 m_0 . Electric-controllable spin-polarization features in the spin texture of monolayer GaSe are predicted. The tunable electronic, optical, and magnetic

properties of monolayer GaSe open up a great prospect for its device applications in both the optoelectronics and spintronics.

ACKNOWLEDGMENTS

We thank Tzu-Cheng Wang and Chunmiao Zhang for their help with the calculations and data analysis. The work was supported by the National Natural Science Foundations of China (Grants No. 61674124, No. 11604275, No. 61774128, No. U1405253, No. 11304257, and No. 11404271), Natural Science Foundation of the Fujian Province of China (Grants No. 2017J01012 and No. 2016J01037), and Fundamental Research Funds for the Central Universities (Grants No. 20720160122, No. 20720160044 and No. 20720170012). C. K. also thanks National Taiwan University for its hospitality during his visits in which parts of this work were carried out.

-
- [1] K. S. Novoselov, V. I. Fal'ko, L. Colombo, P. R. Gellert, M. G. Schwab, and K. Kim, A roadmap for graphene, *Nature (London)* **490**, 192 (2012).
- [2] A. K. Geim and K. S. Novoselov, The rise of graphene, *Nat. Mater.* **6**, 183 (2007).
- [3] K. S. Novoselov, A. K. Geim, S. V. Morozov, D. Jiang, Y. Zhang, S. V. Dubonos, I. V. Grigorieva, and A. A. Firsov, Electric field effect in atomically thin carbon films, *Science* **306**, 666 (2004).
- [4] K. Sengupta and G. Baskaran, Tuning Kondo physics in graphene with gate voltage, *Phys. Rev. B* **77**, 045417 (2008).
- [5] M. Buscema, D. J. Groenendijk, S. I. Blanter, G. A. Steele, H. S. J. van der Zant, and A. Castellanos-Gomez, Fast and broadband photoresponse of few-layer black phosphorus field-effect transistors, *Nano Lett.* **14**, 3347 (2014).
- [6] Y. P. Wu, H. Chou, H. X. Ji, Q. Z. Wu, S. S. Chen, W. Jiang, Y. F. Hao, J. Y. Kang, Y. J. Ren, R. D. Piner, and R. S. Ruoff, Growth mechanism and controlled synthesis of AB-stacked bilayer graphene on Cu-Ni alloy foils, *ACS Nano* **6**, 7731 (2012).
- [7] X. Zhou, L. Gan, W. M. Tian, Q. Zhang, S. Y. Jin, H. Q. Li, Y. Bando, D. Golberg, and T. Y. Zhai, High-mobility Sm-doped Bi₂Se₃ ferromagnetic topological insulators and robust exchange coupling, *Adv. Mater.* **27**, 4823 (2015).
- [8] K. Imai, K. Suzuki, T. Haga, Y. Hasegawa, and Y. Abe, Phase diagram of In-Se system and crystal growth of indium monoselenide, *J. Cryst. Growth* **54**, 501 (1981).
- [9] W. Feng, W. Zheng, W. W. Cao, and P. A. Hu, Back gated multilayer InSe transistors with enhanced carrier mobilities via the suppression of carrier scattering from a dielectric interface, *Adv. Mater.* **26**, 6587 (2014).
- [10] P. A. Hu, Z. Z. Wen, L. F. Wang, P. H. Tan, and K. Xiao, Synthesis of few-layer GaSe nanosheets for high performance photodetectors, *ACS Nano* **6**, 5988 (2012).
- [11] Q. S. Wang, K. Xu, Z. X. Wang, F. Wang, Y. Huang, M. Safdar, X. Y. Zhan, F. M. Wang, Z. Z. Cheng, and J. He, Van der Waals epitaxial ultrathin two-dimensional nonlayered semiconductor for highly efficient flexible optoelectronic devices, *Nano Lett.* **15**, 1183 (2015).
- [12] M. I. D'yakonov and V. I. Perel', *Theory of Optical Spin Orientation of Electrons and Nuclei in Semiconductors*, Optical Orientation: Modern Problems in Condensed Matter Sciences Vol. 8, edited by F. Meier and B. P. Zakharchenya (North-Holland, Amsterdam, 1984), p. 11.
- [13] M. I. Dyakonov, *Spin Physics in Semiconductors*, Springer Series in Solid-State Science Vol. 157, edited by M. I. Dyakonov (Spring-Verlag, Berlin, 2008), p. 1.
- [14] W. Yao, D. Xiao, and Q. Niu, Valley-dependent optoelectronics from inversion symmetry breaking, *Phys. Rev. B* **77**, 235406 (2008).
- [15] Y. Tang, W. Xie, K. C. Mandal, J. A. McGuire, and C. W. Lai, Optical and spin polarization dynamics in GaSe nanoslabs, *Phys. Rev. B* **91**, 195429 (2015).
- [16] L. Huang, Z. H. Chen, and J. B. Li, Effects of strain on the band gap and effective mass in two-dimensional monolayer GaX (X = S, Se, Te), *RSC Adv.* **5**, 5788 (2015).
- [17] Y. H. Lu, C. M. Ke, M. M. Fu, W. Lin, C. M. Zhang, T. Chen, H. Li, J. Y. Kang, Z. M. Wu, and Y. P. Wu, Magnetic modification of GaSe monolayer by absorption of single Fe atom, *RSC Adv.* **7**, 4285 (2017).
- [18] T. Cao, Z. L. Li, and S. G. Louie, Tunable Magnetism and Half-Metallicity in Hole-Doped Monolayer GaSe, *Phys. Rev. Lett.* **114**, 236602 (2015).
- [19] W. X. Feng, G. Y. Guo, and Y. G. Yao, Tunable magneto-optical effects in hole-doped group-IIIa metal-monochalcogenide monolayers, *2D Mater.* **4**, 015017 (2017).
- [20] W. Wei, Y. Dai, C. W. Niu, X. Li, Y. D. Mad, and B. B. Huang, Electronic properties of two-dimensional van der Waals GaS/GaSe heterostructures, *J. Mater. Chem. C* **3**, 11548 (2015).
- [21] Q. H. Liu, L. Z. Li, Y. F. Li, Z. X. Gao, Z. F. Chen, and J. Lu, Tuning electronic structure of bilayer MoS₂ by vertical electric field: A first-principles investigation, *J. Phys. Chem. C* **116**, 21556 (2012).
- [22] G. Kresse and J. Hafner, *Ab initio* molecular-dynamics simulation of the liquid-metal-amorphous-semiconductor transition in germanium, *Phys. Rev. B* **49**, 14251 (1994).
- [23] G. Kresse and J. Furthmüller, Efficient iterative schemes for *ab initio* total-energy calculations using a plane-wave basis set, *Phys. Rev. B* **54**, 11169 (1996).
- [24] G. Kresse and D. Joubert, From ultrasoft pseudopotentials to the projector augmented-wave method, *Phys. Rev. B* **59**, 1758 (1999).
- [25] Y.-S. Kim, K. Hummer, and G. Kresse, Accurate band structures and effective masses for InP, InAs, and InSb using hybrid functionals, *Phys. Rev. B* **80**, 035203 (2009).
- [26] J. P. Perdew, K. Burke, and M. Ernzerhof, Generalized Gradient Approximation Made Simple, *Phys. Rev. Lett.* **77**, 3865 (1996).
- [27] J. Li, C. G. Duan, Z. Q. Gu, and D. S. Wang, Linear optical properties and multiphoton absorption of alkali halides calculated from first principles, *Phys. Rev. B* **57**, 2222 (1998).
- [28] G. Y. Guo, K. C. Chu, D. S. Wang, and C. G. Duan, Linear and nonlinear optical properties of carbon nanotubes from first-principles calculations, *Phys. Rev. B* **69**, 205416 (2004).

- [29] M. Gajdoš, K. Hummer, G. Kresse, J. Furthmüller, and F. Bechstedt, Linear optical properties in the projector-augmented wave methodology, *Phys. Rev. B* **73**, 045112 (2006).
- [30] S. Saha, T. P. Sinha, and A. Mookerjee, Electronic structure, chemical bonding, and optical properties of paraelectric BaTiO₃, *Phys. Rev. B* **62**, 8828 (2000).
- [31] B. C. Luo, X. H. Wang, E. K. Tian, G. W. Li, and L. T. Li, Electronic structure, optical and dielectric properties of BaTiO₃/CaTiO₃/SrTiO₃ ferroelectric superlattices from first-principles calculations, *J. Mater. Chem. C* **3**, 8625 (2015).
- [32] D. Y. Qiu, F. H. da Jornada, and S. G. Louie, Optical Spectrum of MoS₂: Many-Body Effects and Diversity of Exciton States, *Phys. Rev. Lett.* **111**, 216805 (2013).
- [33] J. Heyd, G. E. Scuseria, and M. Ernzerhof, Hybrid functionals based on a screened Coulomb potential, *J. Chem. Phys.* **124**, 219906 (2006).
- [34] W. J. Huang, L. Gan, H. Q. Li, Y. Ma, and T. Y. Zhai, 2D layered group IIIA metal chalcogenides: Synthesis, properties and applications in electronics and optoelectronics, *CrystEngComm* **18**, 3968 (2016).
- [35] A. Koebel, Y. Zheng, J. F. Petroff, M. Eddrief, L. T. Vinh, and C. Sebenne, A transmission electron microscopy structural analysis of GaSe thin films grown on Si (111) substrates, *J. Cryst. Growth* **154**, 269 (1995).
- [36] A. Ramasubramaniam, D. Naveh, and E. Towe, Tunable band gaps in bilayer transition-metal dichalcogenides, *Phys. Rev. B* **84**, 205325 (2011).
- [37] W. Lin, W. Jiang, N. Gao, D. J. Cai, S. P. Li, and J. Y. Kang, Optical isotropization of anisotropic wurtzite Al-rich AlGaN via asymmetric modulation with ultrathin (GaN)_m/(AlN)_n superlattices, *Laser Photonics Rev.* **7**, 572 (2013).
- [38] H. C. Hsueh, G. Y. Guo, and S. G. Louie, Excitonic effects in the optical properties of a SiC sheet and nanotubes, *Phys. Rev. B* **84**, 085404 (2011).
- [39] L. X. Benedict, E. L. Shirley, and R. B. Bohn, Theory of optical absorption in diamond, Si, Ge, and GaAs, *Phys. Rev. B* **57**, R9385 (1998).
- [40] A. Budweg, D. Yadav, A. Grupp, A. Leitenstorfer, M. Trushin, F. Pauly, and D. Brida, Control of excitonic absorption by thickness variation in few-layer GaSe, *arXiv: 1712.06330v1*.
- [41] B. T. Jonker, Y. D. Park, B. R. Bennett, H. D. Cheong, G. Kioseoglou, and A. Petrou, Robust electrical spin injection into a semiconductor heterostructure, *Phys. Rev. B* **62**, 8180 (2000).
- [42] M. Kohda and G. Salis, Physics and application of persistent spin helix state in semiconductor heterostructures, *Semicond. Sci. Technol.* **32**, 073002 (2017).